Shape Characterization of Subdivision Surfaces – Case Studies

K. Karčiauskas [a] Jörg Peters [b,*], U. Reif [c]

[a] *University of Vilnius*

[b] *University of Florida*

[c] *Darmstadt University of Technology*

Abstract

For subdivision surfaces, it is important to characterize local shape near flat spots and points where the surface is not twice continuously differentiable. Applying general principles derived in [PR0x], this paper characterizes shape near such points for the subdivision schemes devised by Catmull and Clark and by Loop. For generic input data, both schemes fail to converge to the hyperbolic or elliptic limit shape suggested by the geometry of the input mesh: the limit shape is a function of the valence of the extraordinary point rather than the mesh geometry. We characterize the meshes for which the schemes behave as expected and indicate modifications of the schemes that prevent convergence to the wrong shape. We also introduce a type of chart that, for a specific scheme, can help a designer to detect early when a mesh will lead to undesirable curvature behavior.

Key words: subdivision surface, curvature, shape

1 Introduction

Due to its conceptual simplicity, generalized subdivision schemes, in particular [CC78] for quadrilaterals and [Loo87] for triangulations, have found their way into most graphics modelling packages for the entertainment industry (see e.g. [DKT98]). By contrast, providers of CAD/CAM software have taken a more cautious approach and to date, we cannot point to a complete design of a high-end surface, such as an exterior car panel or an optical lens, based on standard subdivision algorithms. A common observation is that subdivision initially does a fine

* Corresponding author
Email address: jorg@cise.ufl.edu (Jörg Peters).

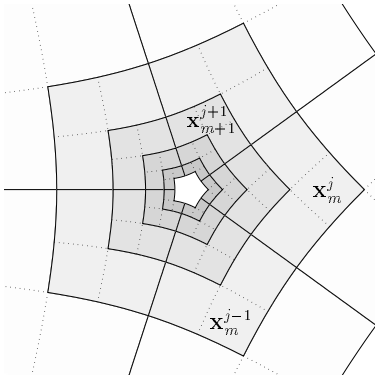

Fig. 1. **Extraordinary points** are the limit points when filling n-sided holes in a surface by an infinite sequence of surface rings.

job in smoothing out transitions between primary surfaces. But in the limit, problems concentrate in the neighborhood of so-called extraordinary points. From the designer's point of view, extraordinary points are associated with mesh nodes that do not have the ordinary number of neighbors, i.e. not 4 neighbors for Catmull-Clark subdivision or not 6 neighbors for Loop's subdivision. For the analysis, extraordinary points are best understood as the limit of a sequence of nested surface rings as illustrated in Figure 1. The problems observed at and near such extraordinary points include unbounded increase of curvature and erratic fluctuation of curvature. It appears that the smoother the ordinary regions are made, the more the shape near extraordinary points deteriorates (see e.g. [ZS01]). A third observation is that subdivision schemes modified to enforce bounded curvature, such as Loop's binary curvature-bounded variant [Loo02] and Sabin's Catmull-Clark variant [Sab91] cause flatness and a concentric wave pattern of the curvature near extraordinary points.

The framework for qualitative shape analysis of subdivision surfaces near extraordinary points developed in [PR0x] allows us to make the statements precise. Applied to the two most widely-used schemes [CC78,Loo87], the analysis reveals intrinsic shape problems near extraordinary points for a wide range of input data. We illustrate the findings for a generic input mesh, shown in Figure 6, where the limit shape drastically differs from the shape of the control structure. We also show how to minimally modify Catmull-Clark to improve at least one of the shape characteristics.

2 Analysis framework near extraordinary points

This section restates the main points of [PR0x]. Let $\mathbf{x}$ be a subdivision surface generated by a stationary, linear and symmetric algorithm. In the vicinity of an extraordinary vertex of valence $n \geq 3$, this surface can be regarded as the union of the extraordinary vertex $\mathbf{m}$ and a sequence of *spline rings* $\mathbf{x}_m$ with domain $\mathbf{S}_n :=$

$\mathbf{\Sigma} \times \mathbb{Z}_n$, where $\mathbf{\Sigma} := [0,2]^2 \setminus [0,1)^2$ (see Figure 1):

$$\mathbf{x}_m : \mathbf{S}_n \to \mathbb{R}^3, \qquad \bigcup_{m\in\mathbb{N}_0} \mathbf{x}_m(\mathbf{S}_n) \cup \mathbf{m} = \mathbf{x}. \tag{1}$$

Here spline is understood in the very general sense as any linear combination of real-valued functions defined on $\mathbf{S}_n$ with weights in $\mathbb{R}^3$, called control points. For example, interpolatory subdivision is considered a spline scheme. Collecting the functions in a row vector g^{t} and the control points in a matrix of three columns $\mathbf{Q}_m$, we have $\mathbf{x}_m = g^{\mathrm{t}}\mathbf{Q}_m$. The sequence of control points is generated by iterated application of a square *subdivision matrix* A to the initial data $\mathbf{Q}_0$. The subdivision matrix has eigenvalues $\lambda_0, \ldots, \lambda_L$ ordered by modulus and (possibly generalized) eigenvectors $v_0, \ldots, v_L$. We define *eigenfunctions* $\psi_\ell := g^{\mathrm{t}} v_\ell$ and write the coefficients of the eigendecomposition of the initial data, $\mathbf{Q}_0 = \sum_{\ell=0}^{L} v_\ell \mathbf{b}_\ell$, as row vectors $\mathbf{b}_\ell \in \mathbb{R}^3$. Then

$$\mathbf{x}_m = g^{\mathrm{t}} A^m \mathbf{Q}_0 = \sum_{\ell=0}^{L} \lambda_\ell^m \psi_\ell \mathbf{b}_\ell, \tag{2}$$

where $\mathbf{x}_m$ is a row vector of three functions.

To analyze shape at an extraordinary point where the limit surface is not necessarily C^2, we make some generic assumptions.
(a) the functions in g^{t} form a partition of unity, and are, at least piecewise, C^2.
(b) The eigenfunctions ψ_ℓ corresponding to $\lambda_\ell \neq 0$ are linearly independent.
(c) $\lambda_0 = 1 > \lambda := |\lambda_1| > \mu := \lambda_3 = \cdots = \lambda_Q > |\lambda_{Q+1}|$ for some $Q \geq 3$.
(d) The *characteristic map* $\mathbf{\Psi} := (\psi_1, \psi_2) : \mathbf{S}_n \to \mathbb{R}^2$ is injective and regular.
(e) The initial data are *generic*: $\operatorname{rank}(\mathbf{b}_i, \mathbf{b}_j, \mathbf{b}_k) = 3, \quad 0 < i \neq j \neq k \leq Q$.

Then the *local coordinate system*

$$\mathbf{m} = \mathbf{b}_0 = \mathbf{0}, \quad \mathbf{e}_1 = \mathbf{b}_1/\|\mathbf{b}_1\|, \quad \mathbf{e}_2 = \mathbf{n} \times \mathbf{e}_1, \quad \mathbf{e}_3 = \mathbf{n} := \frac{\mathbf{b}_1 \times \mathbf{b}_2}{\|\mathbf{b}_1 \times \mathbf{b}_2\|} \tag{3}$$

is well-defined and $\left[\begin{smallmatrix}\mathbf{b}_1\\ \mathbf{b}_2\end{smallmatrix}\right] = \mathbf{L}\left[\begin{smallmatrix}\mathbf{e}_1\\ \mathbf{e}_2\end{smallmatrix}\right]$ for the lower triangular 2×2 matrix $\mathbf{L}$ that orthonormalizes the tangent coordinates. [PR0x] shows that, in this coordinate system,

$$\mathbf{x}_m = \mathbf{x}_{\mathrm{c}} \operatorname{diag}(\lambda^m, \lambda^m, \mu^m) + (o(\lambda^m), o(\lambda^m), o(\mu^m)), \tag{4}$$

$$\mathbf{x}_{\mathrm{c}} := (\mathbf{\Psi}_{\mathrm{c}}, \psi), \qquad \mathbf{\Psi}_{\mathrm{c}} := \mathbf{\Psi}\mathbf{L}, \quad \psi := \sum_{q=3}^{Q} \psi_q \langle \mathbf{b}_q, \mathbf{n}\rangle. \tag{5}$$

The spline ring $\mathbf{x}_{\mathrm{c}} : \mathbf{S}_n \to \mathbb{R}^3$ is called the *central surface* of the subdivision surface $\mathbf{x}$. It depends on the initial data via $\mathbf{b}_q$, but not on the iteration index m. Its Gaussian curvature is abbreviated as K_{c}.

Section 4 of [PR0x] defines three subtly different notions of shape in the vicinity of an extraordinary point where the surface is not necessarily C^2. These can be verified

shape at $\mathbf{m}$	definition	verification
elliptic in sign	exists $\mathcal{N}$: $\mathbf{x} \cap \mathbb{T}_c \cap \mathcal{N} = \mathbf{m}$	$\psi > 0$ or $\psi < 0$
hyperbolic in sign	for all $\mathcal{N}$, $\mathbf{x}$ has points on both sides of $\mathbb{T}_c$	ψ changes sign
elliptic in the limit	exists $\mathcal{N}$: $K > 0$ in $\mathcal{N} \backslash \mathbf{m}$	$K_{\mathrm{c}} > 0$
hyperbolic in the limit	exists $\mathcal{N}$: $K < 0$ in $\mathcal{N} \backslash \mathbf{m}$	$K_{\mathrm{c}} < 0$
hybrid	for all $\mathcal{N}$, K changes sign	K_{c} changes sign
L^2-elliptic	$K_{2,\mathrm{c}} > 0$	$K_{2,\mathrm{c}} > 0$
L^2-hyperbolic	$K_{2,\mathrm{c}} < 0$	$K_{2,\mathrm{c}} < 0$

Fig. 2. Summary of the shape characterizations developed in [PR0x].

based on $\mathbf{x}_{\mathrm{c}}$ and are summarized in Figure 2. The first measures intersections of the subdivision surface with tangent plane $\mathbb{T}_c$ at $\mathbf{m} = 0$ in a sufficiently small neighborhood $\mathcal{N}$ of $\mathbf{m}$. The second measures the Gaussian curvature K of the subdivision surface wherever it is well defined near $\mathbf{m}$. The third measures the *L^2-Gaussian curvature* of the central surface defined as $K_{2,\mathrm{c}} := \det \mathbf{S}$, where $\mathbf{S}$ minimizes $\left\| \psi - \frac{1}{2} \mathbf{\Psi}_{\mathrm{c}} \mathbf{S} \mathbf{\Psi}_{\mathrm{c}}^T \right\|$.

Depending on the input data, any high-quality subdivision scheme should be able to generate elliptic or hyperbolic shape and avoid the hybrid case. A simple way to check for deficiencies of a subdivision scheme is based on the *Fourier index*, $\mathcal{F}(\nu) := \{k \in \mathbb{Z}_n : \nu \text{ is eigenvalue of } \hat{A}^k\}$. The following theorem from [PR0x] implies that high-quality schemes should have a 3-fold third-in-absolute-value-largest, or subsub-dominant eigenvalue with Fourier index $\mathcal{F}(\mu) = \{0, 2, n-2\}$.

Theorem 2.1 *Let $\mathcal{F}$ be the* Fourier index *function and assumptions (a) through (e) hold.*
If $\mathcal{F}(\lambda) \neq \{1, n-1\}$, then the subdivision scheme is not C^1.
If $\mathcal{F}(\mu) \not\subset \{0, 2, n-2\}$, then the subdivision scheme is not C^2.
If $0 \notin \mathcal{F}(\mu)$, then $\mathbf{m}$ is hyperbolic in sign and not L^2-elliptic.
If $\{2, n-2\} \not\subset \mathcal{F}(\mu)$ then $\mathbf{m}$ is not L^2-hyperbolic.

Another shape criterion is well-known and made precise in [PR0x].

Theorem 2.2 *Define $\varrho := \frac{\mu}{\lambda^2}$ and assumptions (a) through (e) hold.*
If $\varrho < 1$, then both principal curvatures converge to 0.
If $\varrho > 1$, then at least one principal curvature diverges.
If $\varrho = 1$, then both principal curvatures are bounded and at least one of them does not converge to 0.

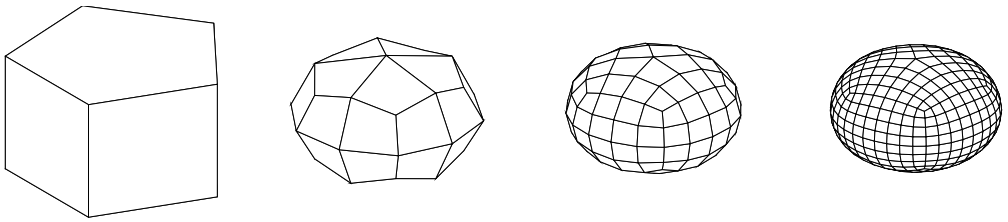

Fig. 3. **Three steps of Catmull-Clark subdivision.** The extruded pentagon features two extraordinary points of valence $n = 5$ and ten of valence $n = 3$.

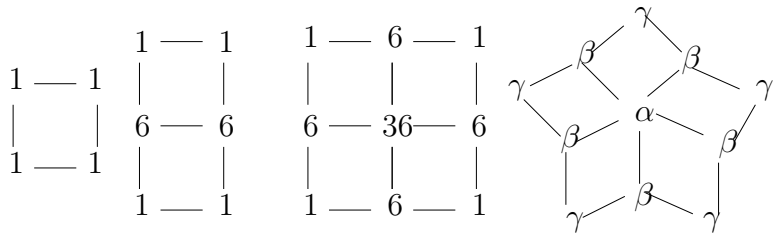

Fig. 4. (Unnormalized) **refinement stencils of generalized Catmull-Clark subdivision**.

3 Catmull-Clark subdivision

We analyze subdivision schemes with stencils of the type displayed in Figure 4. First, we look at the standard Catmull-Clark choices for α and β.

Lemma 3.1 *Let λ_j^i denote the jth largest eigenvalue of the ith Fourier block of the Catmull-Clark subdivision matrix (see Figure 5) and n the valence of the isolated extraordinary point. Then*

$$\begin{aligned}
&\textit{For } n = 3,\ 1 > \lambda := \lambda_1^1 = \lambda_1^{n-1} > \mu := \lambda_1^0 \qquad\quad > \lambda_2^1 = \lambda_2^{n-1} > \dots \\
&\textit{For } n = 4,\ 1 > \tfrac{1}{2} = \lambda_1^1 = \lambda_1^{n-1} \ > \tfrac{1}{4} = \lambda_1^2 = \lambda_1^{n-2} \ = \lambda_1^0 > \dots \\
&\textit{For } n > 4,\ 1 > \lambda := \lambda_1^1 = \lambda_1^{n-1} > \mu := \lambda_1^2 = \lambda_1^{n-2} > \lambda_1^0 > \dots
\end{aligned}$$

Fourier block

Position (by size) in Fourier block

Fig. 5. Notation for **eigenvalues.**

Proof The eigenvalues of Catmull-Clark subdivision are (see e.g. [BS88,BS90,PR98])

$$\begin{aligned}
&\lambda_0^0 = 1,\\
&\lambda_1^0 = \frac{1}{8}(4\alpha - 1 + \sqrt{(4\alpha-1)^2 + 8\beta - 4}),\\
&\lambda_2^0 = \frac{1}{8}(4\alpha - 1 - \sqrt{(4\alpha-1)^2 + 8\beta - 4}),\\
&\lambda_1^k = \frac{1}{16}(c_{n,k} + 5 + \sqrt{(c_{n,k}+9)(c_{n,k}+1)}),\\
&\lambda_2^k = \frac{1}{16}(c_{n,k} + 5 - \sqrt{(c_{n,k}+9)(c_{n,k}+1)}),\\
&\frac{1}{2^l} \text{ for } l = 3,4,5,6 \text{ and } 0,
\end{aligned}$$

where $k > 0$, $\quad c_{n,k} := \cos(2\pi k/n)$, $\quad \alpha := 1 - \frac{7}{4n}$, $\quad \beta := \frac{3}{2n}$ (and $\lambda_0^k = 0$ for $k \neq 0$).

For $n \leq 10$, the statement is checked directly with the help of a symbolic solver. In particular, for $n = 3$, $\lambda_i^1 = \lambda_i^2$ and $\lambda_2^0 = 0 < \lambda_2^1$ and $\mu := \lambda_1^0 := \frac{1}{6} \approx .1667 > .1524 \approx \lambda_2^1 > \frac{1}{8}$. In general, $\lambda_1^1 > \lambda_1^2$ since $c_{n,1} > c_{n,2}$. For $n > 10$, we first show $\lambda_1^0 < \lambda_1^2$,i.e. the third largest eigenvalue by modulus is $\mu = \lambda_1^2$. Since $n(5 + 3\sqrt{5}) > (2\pi)^2(1 + \sqrt{5})$,

$$\begin{aligned}
8\lambda_1^0 &= 3 - \frac{7}{n} + \frac{1}{n}\sqrt{5n^2 - 30n + 49}\\
&\leq 3 + \sqrt{5} - \frac{5 + 3\sqrt{5}}{n} < 3 + \sqrt{5} - (\frac{2\pi}{n})^2(1 + \sqrt{5})\\
&\leq \frac{1}{2}(c_{n,k} + 5 + \sqrt{(c_{n,k}+9)(c_{n,k}+1)}) = 8\lambda_1^2.
\end{aligned}$$

To see that $\mu = \lambda_1^2 > (\lambda_1^1)^2 = \lambda^2$, we observe that for $c := c_{n,1} > 1/2$, $16c\sqrt{c^2+4}) > (c+5)\sqrt{(c+9)(c+1)}$ and therefore

$$16^2\mu = 16(2c^2 + 4 + 2c\sqrt{c^2+4}) > (c + 5 + \sqrt{(c+9)(c+1)})^2 = 16^2\lambda^2.$$

The difference $\mu - \lambda^2$ is monotonically increasing with n. |||

The ordering of eigenvalues shown in Lemma 3.1 together with Theorem 2.2 implies the following.

Corollary 3.1 *For generic input data, and for standard Catmull-Clark subdivision rules*

for $n = 3$, $\mu < \lambda^2$, *i.e. the surface has a flat spot at the extraordinary point. However,* $\rho = \mu/\lambda^2 \approx 0.99$, *i.e. the flatness manifests itself extremely weakly.*

for $n = 4$, $\mu = \lambda^2$ *and the surface is* C^2.

for $n > 4$, $\mu > \lambda^2$, i.e. the surface has at least one divergent curvature near the extraordinary point.

The ordering of eigenvalues shown in Lemma 3.1 together with Theorem 2.1 implies the following.

Corollary 3.2 *For generic input data,*

for $n = 3$, $\mu := \lambda_1^0 > \lambda_2^1 = \lambda_2^{n-1}$, i.e. Catmull-Clark subdivision can not model L^2-hyperbolic surfaces;
for $n = 4$, $\lambda_1^2 = \lambda_1^{n-2} = \lambda_1^0$, i.e. Catmull-Clark subdivision can model both hyperbolic and elliptic shape;
for $n > 4$, $\mu := \lambda_1^2 = \lambda_1^{n-2} > \lambda_1^0$, i.e. Catmull-Clark subdivision can not model elliptic surfaces in the sense of L^2 ellipticity and ellipticity in sign.

We define the scalar ratio

$$\sigma := \frac{\lambda_1^2}{\lambda_1^0}.$$

For $n \geq 4$, the amount by which $\sigma \geq 1$ indicates the level of dominance of the hyperbolic over the elliptic contributions at the subsub-dominant level. The first few numbers are listed in the following table. The maximum is attained at $n = 10$. For $n = 3$, $\lambda_2^1/\lambda_1^0 = .9144$.

n	4	5	6	7	8	9	10	11	12	...
σ	1	1.0547	1.0936	1.1165	1.1285	1.1335	1.1346	1.1332	1.1305	...

Shape 'in the limit' cannot just be decided by looking at the spectrum. The worst shape characterization in the limit is 'hybrid', i.e. the surface erratically alternates between hyperbolic and elliptic shape characteristics. Catmull-Clark subdivision is not hybrid but *consistently* ignores any shape clues from the input geometry: for generic input data, the Gauss curvature is always negative. Only if the designer can make sure that all extraordinary points intended to be hyperbolic (and none intended to be elliptic) are of valence $n > 4$ does Catmull-Clark subdivision deliver the expected shape.

Lemma 3.2 *For generic input data and $n > 4$, the extraordinary point of Catmull-Clark subdivision is* hyperbolic in the limit.

Proof Since the denominator of the Gauss curvature, $\det \mathbf{I}_c$, is positive by regularity, the sign of the Gauss curvature is the sign of the determinant of the second fundamental form $\mathbf{II}_c$ of the central surface $\mathbf{x}_c$. The central surface is parametrized over n segments and each segment consists of three square domain pieces $(1,0)+[0..1]^2$, $(1,1)+[0..1]^2$ and $(0,1)+[0..1]^2$. On each piece, the central surface is a polynomial of bidegree (3,3) and can be expressed in Bézier form. The entries of $\mathbf{II}_c$ are of the form $\det(\partial_s \mathbf{x}_c, \partial_t \mathbf{x}_c, \partial_s \partial_t \mathbf{x}_c)$ for $s, t \in \{u, v\}$ and $\partial_s \mathbf{x}$ the partial derivative of

$\mathbf{x}_c$ with respect to the variable s. Specifically, the entries are the product of partial derivatives of the eigenfunctions corresponding to λ and its sub-dominant eigenvectors v_1, v_2, and of μ and its subsub-dominant eigenvectors v_3, v_4 (c.f. [PU00] Section 3, p 457). The entries are polynomials of bidegree (6,8), (7,7) or (8,6). Therefore $\det \mathbf{II}_c$ has the form

$$\det \mathbf{II}_c(\mathbf{u}) = \sum_{i,j\in\{3,4\}} q_i q_j k_{ij}(\mathbf{u}). \tag{6}$$

where each k_{ij} is a polynomial of bidegree (14,14) and q_i and q_j depend on the eigencoefficients of the decomposition of the input data into the eigenvectors v_k. Since the input data are generic, q_i and q_j are not zero. The quadratic form $\det \mathbf{II}_c$ in q_i and q_j is negative for all nonzero q_i and q_j exactly if the eigenvalues of the symmetric matrix $\left[\begin{smallmatrix} k_{33} & k_{34}/2 \\ k_{34}/2 & k_{44} \end{smallmatrix}\right]$ are negative, i.e. if the function(s)

$$q := k_{33} + k_{44} \pm \sqrt{(k_{33} - k_{44})^2 + k_{34}^2} < 0 \tag{7}$$

on the domain piece. If v corresponds to the kth Fourier block then $v = [\omega^0 \hat{v}, \omega^k \hat{v}, \ldots, \omega^{(n-1)k} \hat{v}]$. Thus, moving from one segment to the next, the entries of $\mathbf{II}_c$ change by ω^4. Distributing this change to q_i and q_j, we see that it suffices to consider one segment of n.

Using range arithmetic for $n = 5, \ldots, 450$, we checked that $k_{33} + k_{44} < 0$ and $(k_{33} - k_{44})^2 + k_{34}^2 < 0$. The calculations are surprisingly subtle in that one cannot just use larger intervals to include several n but has to choose the tightest enclosures of the $\cos(\frac{2\pi j}{n})$-values with 20-digit arithmetic. Of course, valence $n \leq 450$ is more than enough for any practical application but for completeness we argue the case for $n > 450$. If $n > 450$ then $\delta := 1 - \cos(2\pi/n) < 10^{-4}$. Treating each eigenvector $v \in \{v_1, v_2, v_3, v_4\}$ as a function of δ,

$$\begin{gathered} v(1) + \partial_c v(1)\delta + M\delta^2 \;\geq\; v(c) \;\geq\; v(1) + \partial_c v(1)\delta - M\delta^2, \\ M := \max_{\delta\in[0..10^{-4}]} |\partial_c \partial_c v|. \end{gathered}$$

Since $M = |\partial_c \partial_c v(1)|$ and, for $\delta = 0$, $v_1 = v_2$ and $v_3 = v_4$, δ can then be factored out and cancelled so that range arithmetic can then show negativity of the Bézier coefficients of q for $n > 450$. |||

3.1 A sample data set

To illustrate the results, we select the specific, particularly simple symmetric input data shown in Figure 6. The x and y control points are those of the characteristic map of Catmull-Clark subdivision and $z = 1 - x^2 - 2y^2$. This mesh does not hint at a saddle shape. The valence $n = 8$ of the extraordinary point assures that the hyperbolic subsub-dominant terms will be pronounced and the asymmetry in z makes

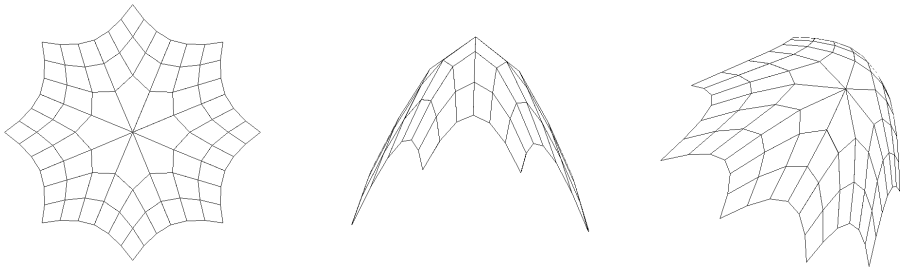

Fig. 6. Three views of the input mesh (8-sided, symmetric in x,y). The **mesh is convex** in the sense that it admits a choice of diagonals that turns it into a convex triangulation (see Figure 14, *left*).

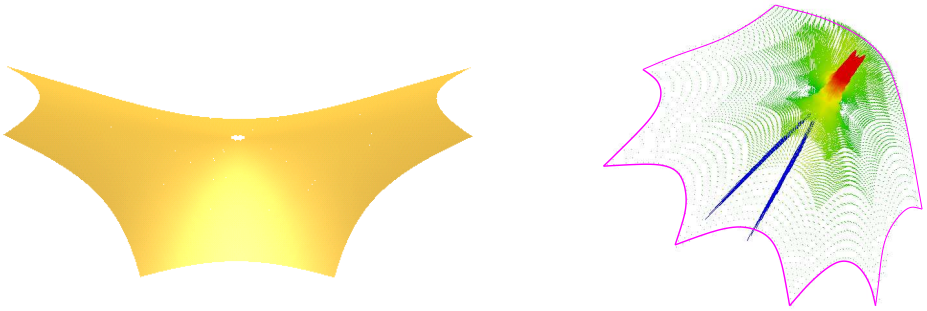

Fig. 7. **Catmull-Clark subdivision applied to the convex mesh** shown in Figure 6. (*left*) Surface rings 24 to 30 scaled 100-fold in the normal direction (up). (*right*) The surface rendered transparent with normal needles in place of surface points. The length of each needle is proportional to the Gauss curvature. The two large downward pointing spikes, below the surface, show the dramatic switch to negative Gaussian curvature in the 5th subdivision step right after a spike in positive Gaussian curvature in the 4th subdivision.

the data generic. Indeed, even though the initial mesh (Figure 6) admits a convex triangulation and the first annulus of patches has positive Gauss curvature, Figure 7, *left*, shows that the surface turns in to a saddle after several steps of subdivision. The lack of convexity becomes apparent after five subdivision steps when the needle plot in Figure 7, *right* reverses orientation. By just looking at a given mesh, it does not appear possible to gauge the magnitude of the eigencoefficients and thus guess what mesh configurations may have a faster or slower onset of hyperbolicity. It is therefore unlikely that designers would develop the skill of manually choosing control points that reduce the shape problem. However, an numerical test against a precomputed chart, as in Section 4, may help.

3.2 Modifying the extraordinary vertex rule of Catmull-Clark subdivision

In this section, we consider modifications of Catmull-Clark subdivision by different choices of α, β and γ so that all three numbers are positive and sum to one. Modifying the weights of the extraordinary vertex rule was already considered, e.g. in [BS90]. The purpose here is to illustrate some of the finer points of the shape analysis, not to devise an overall best scheme to replace Catmull-Clark subdivision on quadrilateral meshes. For finding such an optimal scheme, one would want to additionally modify rules for vertices besides the extraordinary point.

3.2.1 Enforcing $\mu = \lambda^2$ (bounded curvature)

For $n = 3$, solving $\mu = \lambda^2$ for β yields

$$\beta_3^{\text{bd}} := \frac{1}{64}\Big(\frac{13217 + 1017\sqrt{17}}{256} + \alpha(-49 - 9\sqrt{17})\Big). \approx 1.0626 - 1.3454\alpha. \quad (8)$$

Then $\beta < \beta_3^{\text{bd}}$ implies $\mu < \lambda^2$, i.e. a flat spot, $\beta = \beta_3^{\text{bd}}$ yields bounded curvature (hence the superscript ^{bd}) and $\beta > \beta_3^{\text{bd}}$ unbounded curvature. To obtain $\mu = \lambda^2$ and keep both β and γ in $[0..1]$, α is restricted to $0.1813 \le \alpha \le 0.7898$. The standard values, $\alpha = \frac{5}{12}$ and $\beta = \frac{1}{2}$, almost meet the boundedness constraint! The value corresponding to $\alpha = \frac{5}{12}$ should be $\beta_3^{\text{bd}} \approx 0.5020$.

For $n > 4$, $\lambda = \lambda_1^1$ but $\lambda_1^2 = \lambda_1^{n-2}$ do not depend on α and β. Since $\lambda^2 < \lambda_1^2$, we cannot find a subsub-dominant eigenvalue μ such that $\mu = \lambda^2$.

3.2.2 Enforcing triple subsub-dominant eigenvalues (flexibility)

For $n = 3$, solving $\lambda_1^0 = \lambda_2^1$ for β yields

$$\beta_3^{\text{flex}} := \frac{1}{64}\big(117 - 13\sqrt{17} + \alpha(-144 + 16\sqrt{17})\big) \approx .9906 - 1.2192\alpha. \quad (9)$$

Evidently, we cannot enforce both $\mu = \lambda^2$ and $\lambda_1^0 = \lambda_2^1$ simultaneously. To obtain triple subsub-dominant eigenvalues and keep $\beta, \gamma \in [0..1]$, α can vary in $\alpha \in [0 \,..\, 0.8125]$.

For $n > 4$, valid choices are

$$\alpha^{\text{flex}} \in [\underline{\alpha}..\overline{\alpha}], \quad \beta^{\text{flex}} := \frac{1}{32}(16 + 4(1 - 4\alpha)\kappa + \kappa^2), \quad (10)$$

where

$$\kappa := 16\lambda_1^2, \quad \underline{\alpha} := \frac{-16 + 4\kappa + \kappa^2}{16(\kappa - 2)}, \quad \overline{\alpha} := \frac{16 + 4\kappa + \kappa^2}{16\kappa}. \quad (11)$$

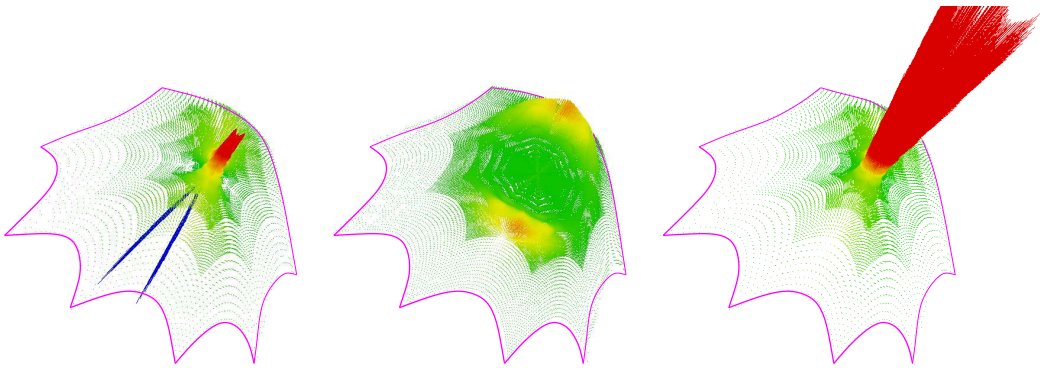

Fig. 8. **Normal needles proportional to Gauss curvature** of (*from left to right*) Catmull-Clark, Sabin's bounded curvature variant [Sab91], the Catmull-Clark variant with $\alpha := (\underline{\alpha} + \overline{\alpha})/2$ applied to the mesh shown in Figure 6. The length of each needle is proportional to the Gauss curvature. The color scale is clamped between -1 and +1 and uniformly distributed from blue to green to red. The bounded curvature variant exhibits a concentric wave-pattern of the Gauss curvature and has a flat plateau.

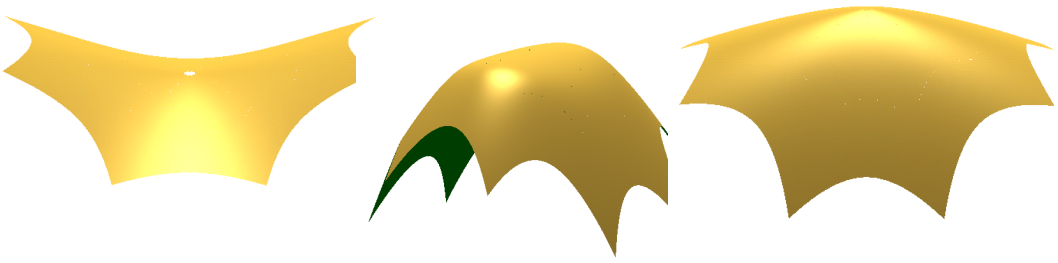

Fig. 9. Rings 24 to 30 of the Catmull-Clark surface (*left*) vs. the Catmull-Clark variant with $\alpha := (\underline{\alpha}+\overline{\alpha})/2$ (*right*), both scaled by 100 in the direction of the normal; (*middle*): flat top of [Sab91] when applied to the mesh shown in Figure 6 (at regular scale).

n	5	6	7	8	9	10	11	12	...
$\underline{\alpha}$	.64247	.73029	.790479	.83333	.86470	.88822	.90624	.92032	...
$\overline{\alpha}$	.77387	.81250	.84718	.87500	.89670	.91362	.92692	.93750	...

The effect of setting $\alpha := (\underline{\alpha}+\overline{\alpha})/2$ is illustrated in Figures 8 and 9. The curvature grows faster than for the standard Catmull-Clark scheme but remains positive as expected. The increasing value of α with n, however, means that the old position of the extraordinary point is weighted ever stronger in determining the new position of the extraordinary point. For higher n this yields undesirable shape.

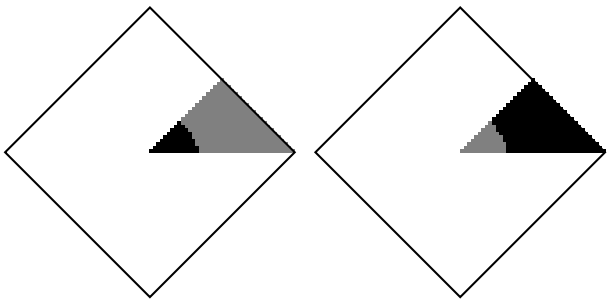

Fig. 10. **Shape characterization charts** for the modified Catmull-Clark scheme with $\alpha := (\underline{\alpha} + \overline{\alpha})/2$, (*left*) *shape in sign*: if $\psi > 0$ or $\psi < 0$ a black pixel is drawn; otherwise a grey pixel. (*right*) L^2 *shape*: grey: $K_{2,\mathrm{c}} > 0$, black: $K_{2,\mathrm{c}} < 0$.

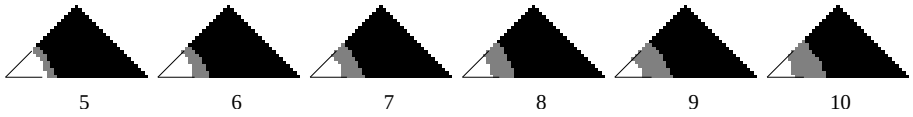

Fig. 11. **Shape-in-the-limit charts** for the modified Catmull-Clark scheme with $\alpha := (\underline{\alpha} + \overline{\alpha})/2$, for valence 5 through 10. Each pixel corresponds to one surface (white: $K_{\mathrm{c}} > 0$, black: $K_{\mathrm{c}} < 0$, grey: hybrid).

4 A technique for characterizing the quality of schemes with triple subsub-dominant eigenvalues

If the spectrum of a scheme is not deficient, but the subdivision matrix has triple subsub-dominant eigenvalues stemming from the correct Fourier blocks then we can analyse its behavior in more detail. The idea is to plot, for each of the three shape characterizations, the shape classification of a representative set of input meshes. Specifically, for each mesh in the representative set of input meshes, we plot a grey, black (or white) pixel according to how the shape characteristic evaluates. The resulting pattern, see Figures 10 and 11, can serve both to prevent a poor choice of mesh for a particular subdivision scheme and, conversely, if the undesirable regions are small, to support the claim that a subdivision scheme is good. At the end of this section, we use diagram 11 to pick out a surface that illustrates hybrid shape-in-the-limit.

For triple subsub-dominant eigenvalues, the central surface can be written as

$$\mathbf{x}_c := (\mathbf{\Psi}_{\mathrm{c}}, \psi), \quad \psi := \sum_{q=3}^{5} \psi_q \langle \mathbf{b}_q, \mathbf{n} \rangle =: a_0\phi_0 + a_2\phi_2 + a_{n-2}\phi_{n-2} \qquad (12)$$

where ϕ_j is the eigenfunction belonging to the jth Fourier block and a_j is the normal component of the eigencoefficient $\mathbf{b}_j$ of the input mesh. Since uniform scaling of the z-direction does not change the shape classification, we may assume, without loss of generality, that $\sum |a_j| = 1$ and $a_0 \geq 0$. Then we can evaluate each

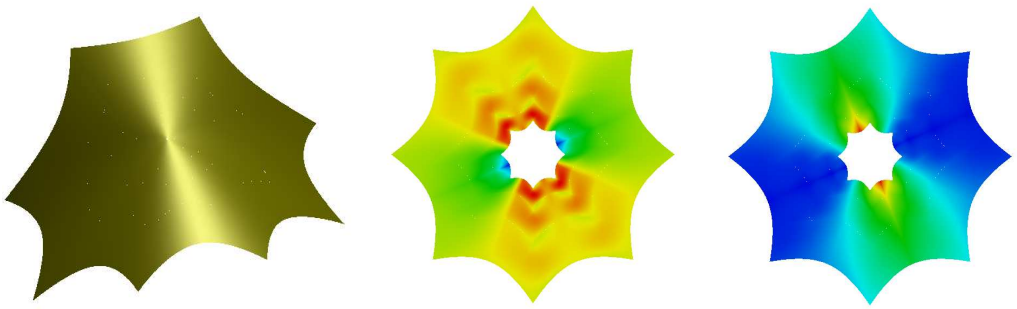

Fig. 12. **Hybrid shape** in the limit of the modified Catmull-Clark scheme with $\alpha := (\underline{\alpha}+\overline{\alpha})/2$ and one input mesh defined by weights $a_0 = 0.6$, $a_2 = 0.2$ and $a_{n-2} = 0.2$. (*from left to right*:) Visible pinchpoint; Gauss curvature; mean curvature.

of the shape characteristics on a rectangular a_2,a_{n-2} grid such that the barycentric coordinate $(a_0, a_2, a_{n-2}) = (1, 0, 0)$ corresponds to the origin.

Off hand the resulting grid covers a diamond-shaped region in the a_2, a_{n-2} space of input meshes. But in our computations, with a grid-spacing of $1/40$, we found the shape classification symmetric with respect to the a_2, a_{n-2} and the $a_2 = a_{n-2}$ axes. (This holds e.g. if, with r the rotation by $\pi/4$, $\phi_{n-2} = \phi_2 \circ r$, $\phi_0 = \phi_0 \circ r$ and $-\phi_2 = \phi_2 \circ r^2$.) Figures 10 and 11 therefore only show the relevant $1/8$th of the diamond, namely the wedge with vertices $(0, 0)$, $(1, 0)$ and $(1/2, 1/2)$.

For *shape in sign*, we converted ψ, for each choice of a_2, a_{n-2}, to Bézier form and subdivided the control mesh twice. If all Bézier coefficients were positive or all were negative, we marked the corresponding pixel black, otherwise grey. The results for $n = 5, \ldots, 10$ are all equal and are shown in Figure 10, *left*.

For L^2-shape, we evaluated each Bézier patch of $\mathbf{x}_c$ on a grid with (u, v) parameter spacing of 0.1 and fit the best quadratic function $f(x, y)$ to the resulting x, y, z values. If the Hessian of f had a positive determinant, we marked the corresponding pixel grey, otherwise black. Again the results for $n = 5, \ldots, 10$ were almost indistinguishable except that the grey region shrinks slowly.

For *shape in the limit*, we evaluated the Gauss curvature of each patch in 16 locations per Bézier patch. If the Gauss curvature was everywhere positive, we marked the corresponding pixel white, if it turned out to be everywhere negative, we marked it black and otherwise, if it was mixed, we marked it grey. This undesirable grey hybrid region grows with n. To illustrate the problem with 'hybrid in the limit' surfaces, we picked one hybrid surface corresponding to $n = 8$, $a_0 = 0.6$, $a_2 = 0.2$ and $a_{n-2} = 0.2$. This surface is shown in Figure 12.

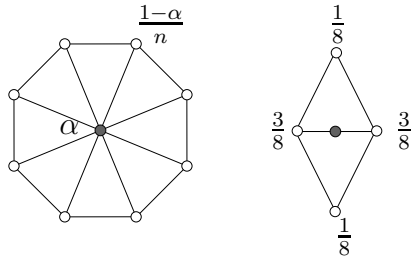

Fig. 13. **Stencils of Loop**'s subdivision scheme. (*left*:) extraordinary point stencil. (*right*:) edge stencil.

5 Loop's subdivision

The analysis of subdivisions with the stencils of Figure 13 is shorter then the earlier analysis of Catmull-Clark-like surfaces. The eigenvalues of Loop's subdivision are $\lambda_0^0 = 1$, $\frac{1}{8}$ (n-fold), $\frac{1}{16}$ (n-fold), 0 ($(4n-1)$-fold) and

$$\lambda_1^0 = \alpha - \frac{3}{8} = \frac{1}{64}(3+2c)^2, \quad 1-\alpha := \frac{5}{8} - \frac{(3+2c)^2}{64},$$
$$\lambda_1^k = \frac{1}{8}(3+2c_{n,k}),\ k>0, \quad c_{n,k} := \cos(2\pi k/n), \text{ and } c := c_{n,1}.$$

Here α is the weight associated with the extraordinary node in the stencil of the extraordinary node.

Lemma 5.1 *Let λ_j^i denote the jth largest eigenvalue of the ith Fourier block of the Loop subdivision matrix.*

$$\begin{aligned}
&\textit{For } n=3, && 1 > \lambda := \lambda_1^1 = \lambda_1^{n-1} = \tfrac{1}{4} > \mu := \tfrac{1}{8} && > \lambda_1^0 = \tfrac{1}{16},\\
&\textit{For } n\in\{4,5\}, && 1 > \lambda := \lambda_1^1 = \lambda_1^{n-1} && > \mu := \lambda_1^0 = \lambda^2 \quad > \lambda_1^2 = \lambda_1^{n-2} \geq \tfrac{1}{8} > \ldots,\\
&\textit{For } n=6, && 1 > \tfrac{1}{2} = \lambda_1^1 = \lambda_1^{n-1} && > \tfrac{1}{4} = \lambda_1^2 = \lambda_1^{n-2} \quad = \lambda_1^0 > \tfrac{1}{8} > \ldots\\
&\textit{For } n>6, && 1 > \lambda := \lambda_1^1 = \lambda_1^{n-1} && > \mu := \lambda_1^2 = \lambda_1^{n-2} > \lambda_1^0 > \tfrac{1}{8} > \ldots.
\end{aligned}$$

Proof For all n, $\lambda_1^1 > \frac{1}{8}$ and $\lambda_1^1 > \lambda_1^0 = (\lambda_1^1)^2$ and $\lambda_1^1 > \lambda_1^k$ for $k > 1$. The difference

$$64(\lambda_1^2 - \lambda_1^0) = 8(3+2(2c^2-1)) - (3+2c)^2 = (14c+1)(2c-1)$$

implies that

$$\begin{aligned}
&\text{for } n=3: && \tfrac{1}{8} > \lambda_1^0 = \tfrac{1}{16},\ (\lambda_1^2 = \lambda_1^{n-1} = \lambda_1^1),\\
&\text{for } n=4,5: && \lambda_1^0 > \lambda_1^2 \qquad (\lambda_1^2 \geq \tfrac{1}{8}),\\
&\text{for } n>6: && \lambda_1^2 > \lambda_1^0 \qquad (\lambda_1^0 > \tfrac{1}{4}).
\end{aligned}$$

For $n > 6$, $c > 1/2$ and therefore

$$64(\mu - \lambda^2) = 8(3 + 2(2c^2 - 1)) - (3 + 2c)^2 = 28c^2 - 12c - 1 > 0,$$

increasing with n. |||

The ordering of eigenvalues shown in Lemma 5 together with Theorem 2.2 implies that, for generic input data,

valence	$\rho = \frac{\mu}{\lambda^2}$	curvature near the extraordinary point
3	> 1	divergent
4,5,6	$= 1$	bounded
> 6	> 1	divergent

The ordering of eigenvalues shown in Lemma 5 together with Theorem 2.1 implies the following table for generic input data. For $n = 3$, the hyperbolic terms come from lower Fourier components.

valence		shape
3	3-fold $\mu := \frac{1}{8}$	one from each Fourier component
4,5	$\mu = \lambda_1^0 > \lambda_2^1 = \lambda_2^{n-1}$	can not model L^2-hyperbolic surfaces.
6	$\mu = \lambda_1^0 = \lambda_2^1 = \lambda_2^{n-1}$	can model hyperbolic and elliptic surfaces.
> 6	$\mu = \lambda_2^1 = \lambda_2^{n-1} > \lambda_1^0$	can not model L^2-elliptic and surfaces elliptic in sign.

For $n = 4$, we get $\frac{9}{64} = \lambda_1^0 \approx \lambda_1^2 = \frac{8}{64}$. For $n = 5$, we get $\lambda_1^0 - \lambda_1^2 = \frac{\sqrt{5}(13-5\sqrt{5})}{128} \approx 2.4834 \cdot 10^{-4}$. That is, for $n = 4$ and $n = 5$, the ratio $\sigma \approx 1$. While the curvatures are dominated by the elliptic term, the hyperbolic terms are only slightly smaller. This explains why the lack of flexibility would not easily be observed when only a few iterations of the algorithm are used.

The ratio $\sigma = \lambda_1^2/\lambda_1^0$ is monotonically increasing with n but has a supremum of only 1.6. Therefore, if the mesh has a large eigencomponent corresponding to λ_1^0 and a small one corresponding to λ_1^2 and λ_1^{n-2}, the onset of hyperbolic dominance may only occur after many iterations. This is exactly the case when we triangulate the mesh of Figure 8 by inserting quad-bisectors in a circular fashion around the extraordinary node as shown in Figure 14, *left*. We record (with Maple's 20-digit arithmetic) a sequence of convex surface rings up to subdivision level 17. From level 18 onwards, a 'channel' of negative, and fast decreasing Gauss curvature appears.

Finally, we can determine α to obtain the full complement of subsub-dominant eigenvectors for $n > 3$, i.e. to have $\lambda_1^2 = \lambda_1^0$. However, the solution, $\alpha^{\text{flex}} :=$

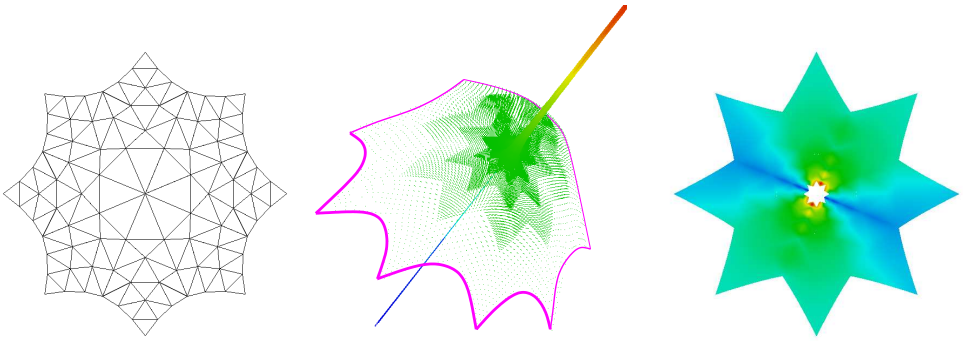

Fig. 14. (*left:*) **Convex triangulation** of the quad-mesh in Figure 8. (*middle:*) Curvature needle plot confirms late, but certain dominance of negative terms in **Loop's** scheme. (*right:*) Channel of negative curvature visible in subdivision levels 17–20.

$(1 + c^2)/2$, increases quickly with n; that is, the weight of the extraordinary node increases, rather than decreases, as the number of neighbors increases and the resulting surfaces show an undesirable curvature distribution.

Acknowledgement: This research was supported by the grant NSF 9457806-CCR. We thank Malcolm Sabin for commenting on a preprint. The curvature textures and needle plots were generated were generated with the OpenGL-based *bview* package [WP].

References

[BS88] A. A. Ball and D. J. T. Storry. Conditions for tangent plane continuity over recursively generated B-spline surfaces. *ACM Trans. on Graphics*, 7:83–102, 1988.

[BS90] A. A. Ball and D. J. T. Storry. An investigation of curvature variations over recursively generated B-spline surfaces. *ACM Transactions on Graphics*, 9(4):424–437, October 1990.

[CC78] E. Catmull and J. Clark. Recursively generated B-spline surfaces on arbitrary topological meshes. *Computer-Aided Design*, 10:350–355, September 1978.

[DKT98] T DeRose, M Kass, and T Truong. Subdivision surfaces in character animation. In Michael Cohen, editor, *SIGGRAPH 98 Conference Proceedings*, Annual Conference Series, pages 85–94. ACM SIGGRAPH, Addison Wesley, July 1998. ISBN 0-89791-999-8.

[Loo87] C.T. Loop. Smooth Subdivision Surfaces Based on Triangles. Master's thesis, Department of Mathematics, University of Utah, August 1987.

[Loo02] Charles Loop. Bounded curvature triangle mesh subdivision with the convex hull property. *The Visual Computer*, 18:316–325, 2002.

[MSI03] M.F. Hassan M.A. Sabin, N.A. Dodgson and I.P. Ivrissimtzis. Curvature behaviours at extraordinary points of subdivision surfaces. *Computer Aided Design*, 35(11):1047–1051, September 2003.

[PR98] J. Peters and U. Reif. Analysis of generalized B-spline subdivision algorithms. *SIAM Journal on Numerical Analysis*, 35(2):728–748, April 1998.

[PR0x] J. Peters and U. Reif. Shape characterization of subdivision surfaces – basic principles. *Computer Aided Geometric Design*, x(x):xx–xx, 200x.

[PU00] J. Peters and G. Umlauf. Gaussian and mean curvature of subdivision surfaces. In R. Cipolla and R. Martin, editors, *The Mathematics of Surfaces IX*, pages 59–69. Springer, 2000.

[Sab91] M Sabin. Cubic recursive division with bounded curvature. In L.L. Schumaker P.J. Laurent, A. LeMéhauté, editor, *Curves and Surfaces*, pages 411–414. Academic Press, 1991.

[WP] X. Wu and J. Peters. bview. http://www.cise.ufl.edu/research/SurfLab/bview.

[ZS01] D Zorin and P Schröder. A unified framework for primal/dual quadrilateral subdivision schemes. *Comput. Aided Geom. Design*, 18(5):429–454, 2001.